W. Wiegmann, Phys. Rev. B 25, 7867 (1982).
[9]N. W. Ashcroft and N. D. Mermin, *Solid State Physics* (Holt, Rinehart and Winston, New York, 1976), Chap. 23.
[10]D. Pines, *Elementary Excitations in Solids* (Benjamin, New York, 1977).
[11]E. Gornik and D. C. Tsui, Solid State Electron. 21, 139 (1977).
[12]P. M. Platzmann and P. A. Wolff, *Waves and Interactions in Solid State Plasmas* (Academic, New York, 1973).
[13]W. Müller, F. Kohl, H. Partl, and E. Gornik, Solid State Electron. 21, 235 (1978).
[14]E. Gornik, Phys. Rev. Lett. 29, 575 (1972).

Observation of Heavy-Ion–Induced Wake-Potential Interference Effects

H. J. Frischkorn, K. O. Groeneveld, P. Koschar, R. Latz, and J. Schader
Institut für Kernphysik der J. W. Goethe-Universität, D-6000 Frankfurt am Main, Germany
(Received 27 September 1982)

The superposition of the wake potentials of Coulomb-exploding fragments of diatomic molecular projectiles penetrating a solid cause potential oscillations at the surface. The total electron yield per projectile serves as a signal to detect these oscillations. The plasma frequency of the solid and the wake-potential wavelength can be deduced from the data.

PACS numbers: 79.20.Rf, 34.90.+q

Energetic ions penetrating solids induce a cylindrically symmetric wake of electron-density fluctuations behind the projectile.[1] The damped periodic potential Φ corresponding to these charge-density fluctuations is characterized by the charge Z_p and the velocity v_p of the projectile and by the dielectric function $\epsilon(\omega_p)$ with the plasma frequency ω_p of the solid.[2,3] Its wavelength λ_w is given by $\lambda_w = 2\pi v_p/\omega_p$. The influence of the charge-density fluctuations and their potential $\Phi(Z_p, v_p, \epsilon)$ on the spectra of secondary electrons has been discussed previously[4-6] and the electron ejection of the solid has been predicted.[4,6]

These calculations prompted our previous experiments[7] where we studied the angular and energy distributions of low-energy ($E_e < 50$ eV) electrons emitted from solids under energetic heavy-ion impact. The observed irregularities in the electron energy and angular distributions coincided with structures predicted by theory.[4,6] However, these results were inconclusive because of large experimental uncertainties.

In a novel approach to find the influence of the wake potential Φ on electron emission from solids we measured the total (i.e., integrated over all emission angles and energies) electron emission per projectile (γ) from solids (carbon). At equal velocities (isotachic) we compare the yields produced by monoionic projectiles C^+ and O^+ [γ(C) and γ(O)] with the yield produced by the molecular projectile CO^+ [γ(CO)] and calculate the ratio $R = \gamma(\mathrm{CO})/[\gamma(\mathrm{C}) + \gamma(\mathrm{O})]$. The ratio R is measured as a function of a quantity r_x/λ_w (see below) which is roughly proportional to t^2 where t is the dwell time $t = x/v_p$ of the projectile in the target with thickness x. A molecular-ion effect is observed if $R(r_x/\lambda_w) \neq 1$. Since most phenomena associated with v_p are monotonic functions of v_p in the velocity range of interest here we can vary either x or v_p.

The experimental setup is shown in Fig. 1. The basic idea is fairly simple, and the equipment inexpensive and quite appropriate to the present poor state of the world economy: Projectiles C^+, O^+, and CO^+ with $1.5 \times 10^{+8} \leq v_p \leq 4 \times 10^{+8}$ cm/s are produced in a 2.5-MV Van de Graaff acceler-

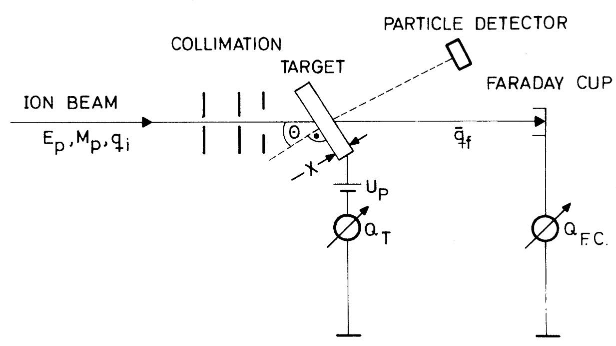

FIG. 1. Schematic presentation of the experimental setup. The symbols are explained in the text. In the present experiment the angle $\theta = 0°$.

ator. After collimation the beam penetrates thin carbon targets (areal density ρx; $2 \leq \rho x \leq 15\ \mu g/cm^2$) and is stopped in a Faraday cup. The charges at the target Q_T and the Faraday cup Q_{FC} are recorded. The charge balance in the intersection of the beam with the target allows us to calculate the total electron yield $\gamma = \bar{q}_f Q_T / Q_{FC} - (q_i - \bar{q}_f)$ where q_i is the charge state of the incident projectile and $\bar{q}_f$ the mean charge state of the emerging projectiles.[8] A voltage U_p could be applied to the target to compensate contact potentials. The charge distributions of the emerging C and O particles from incident C^+, O^+, and also CO^+ projectiles were measured. The mean charge state $\bar{q}_f$ of the emerging particles calculated from these distributions did not deviate within experimental errors of ± 7% from mean charge states calculated from published distributions.[9]

Carbon targets were used throughout the experiment because (1) they are self-supporting and readily available in the desired thickness range; (2) damage of the foils during beam exposure was found to be not serious; (3) under the available vacuum conditions (~10^{-7} Torr) thickness changes during bombardment are likely to add only carbon. The absolute ρx values were measured by Rutherford scattering (see Fig. 1, surface-barrier detector at an angle of 10°) with experimental errors on the order of ± 5%. Possible changes during beam exposure were also monitored by the Rutherford scattering so that relative thickness changes $\Delta x/x$ were known to be < 3%. The thickness $x = \rho x/\rho$ was calculated with $\rho = 1.90$ g/cm^3 (Kennedy, Youngblood, and Blaugrund[10]) and yielded the dwell time $t = x/v_p$ of projectile in the target.

The experimental results of four carbon target thicknesses are presented in Fig. 2. Here, the isotachic ratio $R = \gamma(CO)/[\gamma(C) + \gamma(O)]$ is plotted versus $r_x/\lambda_w = r_x \omega_p t/(2\pi x)$; the quantity $r_x = r_x(t)$ represents the distance of the molecular fragments at the exit surface (see below). The following properties can be stated: (1) $R(r_x/\lambda_w) \neq 1$ for most (r_x/λ_w) values. (2) $R(r_x/\lambda_w) \leq 1$. (3) $R(r_x/\lambda_w)$ oscillates. (4) The amplitude of the oscillations is damped and approximated by a function $R = A + B(x)\sin(r_x/\lambda_w + \varphi)$, for each target thickness where A, B, and φ are fit parameters. (5) The wavelength of the oscillation and A are independent of the target thickness. (6) For thin targets the phase φ equals zero; the phase is found to be $\varphi > 0$ for thicker targets.

The tentative interpretation of the observed R oscillations is based on the periodic fluctuations of the electron density near the surface of the solid caused by the superposition of the wake potentials Φ_1 and Φ_2 of the two fragments of the molecular projectile. The plasma frequency ω_p [$= (21.4\ \text{eV})/\hbar$ for carbon[11]] and v_p determine the

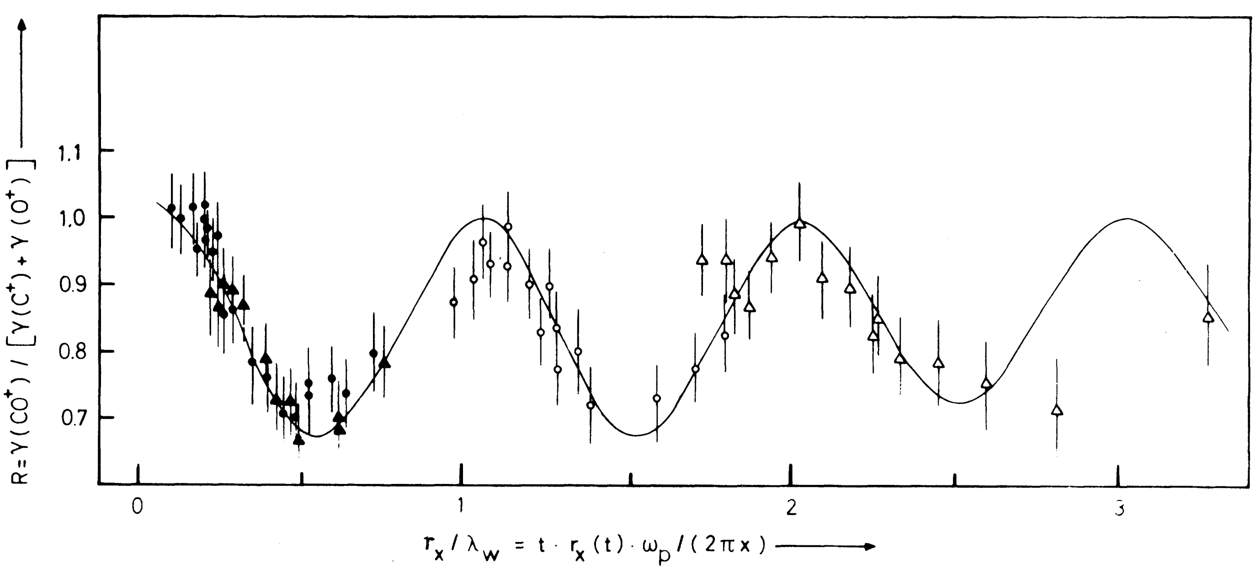

FIG. 2. Total electron yield ratio $R = \gamma(CO)/[\gamma(C) + \gamma(O)]$ vs r_x/λ_w for carbon targets. The solid line is a fit of $R_{fit} = A + B\sin(r_x/\lambda_w + \varphi)$ with $\omega_p = (23\ \text{eV})/\hbar$. The fit parameters of the different target thicknesses are as follow: $\rho x = 2\ \mu g/cm^2$ (filled circles), $B = -0.3$, $\varphi = 0$; $\rho x = 5\ \mu g/cm^2$ (filled triangles), $B = -0.3$, $\varphi = 0$; $\rho x = 8\ \mu g/cm^2$ (empty circles), $B = -0.3$, $\varphi = 0.5$; $\rho x = 12\ \mu g/cm^2$ (empty triangles), $B = -0.25$, $\varphi = 0.7$.

wake wavelength $\lambda_w = 2\pi v_p/\omega_p$ of the wake potential $\Phi(Z_p, v_p, \epsilon(\omega_p))$ (see, e.g., Ref. 3).

After having lost their outer electrons when entering the solid the two fragments of the molecular ion separate very violently (Coulomb explosion[3]). The trajectories of the two fragments [charges $\bar{q}_1^s$ and $\bar{q}_2^s$, reduced mass μ, and bond length, i.e., internuclear separation before entering the solid $r_0 = r(t \leq 0) = 1.13$ Å] inside the solid are described by the equation of motion $\mu\ddot{r}(t) = \bar{q}_1\bar{q}_2 e^2/r^2(t)$. It allows us to calculate the internuclear separation $r_x = r(x = v_p t)$ of the two fragments after the dwell time t at the exit surface. The charges $\bar{q}_1$ and $\bar{q}_2$ inside the solid are approximated by the charges deduced from energy-loss experiments in solids [Eq. (13) in Andersen and Ziegler[12]]. Constructive interference of the two wake potentials Φ_1 and Φ_2 near the surface will occur when $r_x/\lambda_w = n$ (with $n = 0, 1, 2, 3, \ldots$), and destructive interference when $r_x/\lambda_w = (n + \frac{1}{2})$.

Very different mechanisms can contribute to the ion-induced electron emission from solids[4-6,13,14] such as, e.g., kinetic emission, potential emission, or electron emission from heavy-ion–induced collectively excited solids. Generally, three parts can be distinguished: (1) electron production somewhere inside the solid or in the surface; (2) transport of the electrons to the surface; and (3) transmission of the electrons through the surface. Part 3 is particularly sensitive to potential changes at the surface caused, e.g., by the wake potential.

In the framework of these considerations Fig. 2 can qualitatively and—in part—quantitatively be explained as follows:

(1) $R(r_x/\lambda_w) \neq 1$ for most r_x/λ_w values indicates a distinct molecular effect.

(2) $R(r_x/\lambda_w) \leq 1$. An additional negative potential caused by the constructive interference of the exploding molecular fragments at the surface does not increase the yield γ since a saturation is already reached at ~ 30 V. A reduction of the negative potential, however, caused by destructive interference reduces the emission considerably ($B < 0$).[15]

(3) The $R(r_x/\lambda_w)$ oscillations have a wavelength of $r_x/\lambda_w = 1$. This allows calculation of (a) the plasma frequency independently as $\omega_p = (23\ \mathrm{eV})/\hbar$ in reasonable agreement with other methods[11] and (b) the wake wavelength $\lambda_w = 2\pi v_p/\omega_p = 6.7$ Å at, e.g., $v_p = 3.7 \times 10^8$ cm/s.

(4) Both increasing straggling and an increasing mismatch of the wake-potential amplitudes leads to a reduction of the destructive interference minima at increasing r_x/λ_w values. For $r_x \gg \lambda_w$ the damping parameter B decreases.

(5) The plasma frequency of carbon determines the wavelength of the r_x/λ_w oscillations. Therefore, this wavelength and the parameter A are found to be independent of the carbon target thickness.

(6) Since the target thickness uncertainty Δx of thicker targets approaches the wake wavelength λ_w a phase shift φ can be expected and is indeed observed for thicker targets ($\varphi \neq 0$).

(7) It is interesting to note that the first data in Fig. 2 occur only at $r_x/\lambda_w > 0.15$ values: The Coulomb explosion starts not at $r(t=0) = 0$ but at $r(t=0) = r_0 = 1.13$ Å. The wake wavelength of the highest velocity data is $\lambda_{w,\max} = 8.21$ Å; thus $r_x/\lambda_w = r_0/\lambda_{w,\max} = 0.14$, in agreement with the experimental observation.

Concluding, a strong effect of the interference of wake potentials on secondary electron emission has been observed. The molecular ion serves as a tool to probe dynamic properties of the solid in the range of a few angstroms. Thus the wake-potential wavelength and the plasma frequency of the target material can be deduced. The effect of wake-potential interferences on the convoy electron emission will be discussed elsewhere.[16]

Encouraging discussions and helpful suggestions from W. Greiner, I. A. Sellin, U. Gerhard, W. Scheid, and Y. K. Kim are gratefully acknowledged. This work was supported in part by the Bundesministerium für Forschung und Technologie, Bonn, and in part by the Gesellschaft für Schwerionenforschung, Darmstadt.

[1]N. Bohr, K. Dan. Vidensk. Selsk., Mat. Fys. Medd. 18, 8 (1948).

[2]J. Neufeld and R. H. Ritchie, Phys. Rev. 98, 1632 (1955).

[3]Z. Vager and D. S. Gemmell, Phys. Rev. Lett. 37, 1352 (1976).

[4]D. K. Brice and P. Sigmund, K. Dan. Vidensk. Selsk., Mat. Fys. Medd. 48, 8 (1980).

[5]V. N. Neelavathi, R. H. Ritchie, and W. Brandt, Phys. Rev. Lett. 33, 302 (1974).

[6]W. Schäfer, H. Stöcker, B. Müller, and W. Greiner, Z. Phys. A 283, 349 (1978), and B 36, 319 (1980).

[7]H. J. Frischkorn, K. O. Groeneveld, S. Schumann, R. Latz, G. Reichhardt, J. Schader, W. Kronast, and R. Mann, Phys. Lett. 76A, 155 (1980); H. J. Frischkorn, K. O. Groeneveld, S. Schumann, J. Schader,

G. Astner, S. Hultberg, L. Lundin, R. Ramanujam, R. Didriksson, P. Håkansson, B. Sundquist, and R. Mann, in *Inner Shell and X-Ray Physics of Atoms and Solids*, edited by D. J. Fabian, H. Kleinpoppen, and L. M. Watson (Plenum, New York, 1981), p. 193.

[8]J. Schader, B. Kolb, K. D. Sevier, and K. O. Groeneveld, Nucl. Instrum. Methods 151, 563 (1978).

[9]J. B. Marion and F. C. Young, *Nuclear Reaction Analysis* (North-Holland, Amsterdam, 1968).

[10]E. F. Kennedy, D. H. Youngblood, and A. E. Blaugrund, Phys. Rev. 158, 897 (1967).

[11]G. J. Kumbartzki, H. Neuburger, H. P. Kohl, and W. Polster, Nucl. Instrum. Methods 194, 291 (1982).

[12]R. H. Andersen and J. F. Ziegler, *The Stopping and Ranges of Ions in Matter* (Pergamon, New York, 1977), Vol. 5, p. 12.

[13]W. Meckbach, in *Beam Foil Spectroscopy*, edited by I. A. Sellin and D. J. Pegg (Plenum, New York, 1975), p. 577.

[14]D. Hasselkamp, A. Scharmann, and N. Stiller, Nucl. Instrum. Methods 168, 579 (1980); G. Holmén, B. Svenson, J. Schou, and P. Sigmund, Phys. Rev. B 20, 2247 (1979).

[15]H. J. Frischkorn, K. O. Groeneveld, J. Schader, R. Latz, and R. Mann, in Proceedings of the First European Conference on Atomic Physics, Heidelberg, Federal Republic of Germany, 1981, edited by J. Kowalski, G. zu Putlitz, and H. G. Weber (unpublished), p. 822; H. J. Frischkorn, P. Koschar, R. Latz, J. Schader, K. O. Groeneveld, F. Bömmel, G. Saemann-Ischenko, and W. Schmidt, Verh. Dtsch. Phys. Ges. 17, 355 (1982).

[16]R. Latz, H. J. Frischkorn, K. O. Groeneveld, P. Koschar, and J. Schader, to be published.

Localization and Electron-Electron Interaction Effects in Submicron-Width Inversion Layers

R. G. Wheeler, K. K. Choi, A. Goel, R. Wisnieff, and D. E. Prober

Section of Applied Physics, Becton Center, Yale University, New Haven, Connecticut 06520

(Received 29 September 1982)

The localization and electron-electron interaction parts of the small conductivity variation with temperature have been extracted from data obtained on narrow field-effect transistors. One-dimensional behavior is observed and is compared with measurements on the two-dimensional region of the test samples. Magnetoconductance which selectively removes the localization part of the resistance has allowed a theoretical interpretation of the total temperature dependence.

PACS numbers: 71.55.Jv, 72.15.Lh, 73.40.Qv

The interpretation of magnetoconductance measurements performed on two-dimensional silicon inversion layers has been a significant triumph of localization theory.[1,2] By comparison with a scale set by a magnetic length $l_B = (\hbar/2eB)^{1/2}$, experiments have deduced the electron diffusion length between inelastic collisional events, a quantity which previously has been difficult to measure with such directness.[3,4] Concurrently, the calculation of perturbative corrections to the conductivity showed that small conductivity variations will arise of form similar to that predicted by localization considerations. The exchange and Hartree contributions making up this electron-electron interaction nearly cancel each other for the case of short-range impurity potentials applicable to inversion layers.[1] Thus, in comparison with localization the interaction effect is small.[5] In the transition from two dimensions to one dimension,[1] phase-space considerations prevent this near cancellation. Hence there is a high likelihood that both phenomena will be significant. We report observations on quasi one-dimensional silicon inversion layers where both contributions to the small conductivity changes are comparable and distinguishable by magnetoconductance measurements.

Long but narrow metal-oxide-semiconductor field-effect transistors (MOSFETs) have been fabricated where the width is comparable to l_{in}, the inelastic length. That such a structure ought to exhibit one-dimensional localization behavior can be seen by examining the theoretical expression for the weak-localization conductance applicable at a finite temperature,[6]

$$\delta\sigma = -\frac{Se^2}{\pi\hbar}\,\frac{D}{LW}\sum_{q_x}\sum_{q_y}\frac{1}{(Dq^2 + 1/\tau_{\mathrm{in}})}. \qquad (1)$$

Here L and W are the length and width, respectively, of the sample, τ_{in} is the inelastic time,